ADVANCED HEALTHCARE MATERIALS
www.advhealthmat.de

Quantitative and Multiplex Detection of Extracellular Vesicle-Derived MicroRNA via Rolling Circle Amplification within Encoded Hydrogel Microparticles

*Dana Al Sulaiman, Nidhi Juthani, and Patrick S. Doyle**

Extracellular vesicle-derived microRNA (EV-miRNA) represent a promising cancer biomarker for disease diagnosis and monitoring. However, existing techniques to detect EV-miRNA rely on complex, bias-prone strategies, and preprocessing steps, making absolute quantification highly challenging. This work demonstrates the development and application of a method for quantitative and multiplex detection of EV-miRNA, via rolling circle amplification within encoded hydrogel particles. By a one-pot extracellular vesicle lysis and microRNA capture step, the bias and losses associated with standard RNA extraction techniques is avoided. The system offers a large dynamic range (3 orders of magnitude), ease of multiplexing, and a limit of detection down to 2.3 zmol (46×10^{-18} M), demonstrating its utility in clinical applications based on liquid biopsy tests. Furthermore, orthogonal measurements of EV concentrations coupled with the direct, absolute quantification of miRNA in biological samples results in quantitative measurements of miRNA copy numbers per volume sample, and per extracellular vesicle.

1. Introduction

MicroRNA (miRNA)[1,2] are short noncoding RNA that have emerged as highly promising diagnostic and prognostic biomarkers due to their gene regulatory functions and dysregulated patterns in many diseases including cancer.[3–9] miRNAs can exist in various forms in biological fluids[10,11] including freely circulating, bound to proteins, or packaged within extracellular vesicles (EVs).[12–14] EV-miRNAs are particularly attractive biomarkers due to their enhanced stability – resisting degradation by RNAse enzymes. EVs themselves have been implicated in a variety of biological functions, including disease progression, drug resistance, and can act as a form of intercellular communication.[15–18] The contents within exosomes and other microvesicles are actively exported by the parent cells, and as such, EV-miRNA detection could offer insights into disease conditions associated with the parent cells, while being easily accessible from bodily fluids such as serum and urine.[19–22]

While promising, absolute quantification of miRNA is difficult due to their short lengths, high sequence homology among family members, and variable expression levels in biological samples.[23,24] Traditional strategies for miRNA detection, including reverse-transcription qPCR[7] and microarrays,[25] offer limited multiplexing and involve complex multistep procedures. Moreover, RNA isolation from EVs can introduce loss and bias, that can confound interpretation of results.[26] While some studies have demonstrated EV-miRNA profiling in a range of biofluids, differences in RNA and EV isolation in addition to difficulties in data normalization make comparisons with other studies and quantification difficult.[21,26–28] Other studies have also detected EV-miRNA directly from isolated EVs,[29–34] however the demonstrated multiplexing ability is limited. There is thus a pressing need to develop techniques for absolute EV-miRNA quantification to advance fundamental research into their function and to develop diagnostic and prognostic assays for clinical use.

Our group has developed nonfouling hydrogel microparticles, which are compatible with a variety of complex samples, facilitating direct miRNA detection from serum, cell lysate, and formalin-fixed paraffin-embedded (FFPE) tissue sections.[35–37] These particles demonstrate favorable solution kinetics for RNA hybridization and are synthesized using a technique called stop-flow lithography, enabling graphically-encoded multiplexing.[38–40] Utilizing the benefits of hydrogel microparticles for miRNA detection, this work presents a facile and sensitive technique for multiplexed detection of EV-miRNAs. After

D. Al Sulaiman, N. Juthani, P. S. Doyle
Department of Chemical Engineering
Massachusetts Institute of Technology
Cambridge, MA 02142, USA
E-mail: pdoyle@mit.edu
D. Al Sulaiman
Division of Physical Science and Engineering
King Abdullah University of Science and Technology
Thuwal 23955-6900, Kingdom of Saudi Arabia
P. S. Doyle
Harvard Medical School Initiative for RNA Medicine
Boston, MA 02115, USA

The ORCID identification number(s) for the author(s) of this article can be found under https://doi.org/10.1002/adhm.202102332

DOI: 10.1002/adhm.202102332

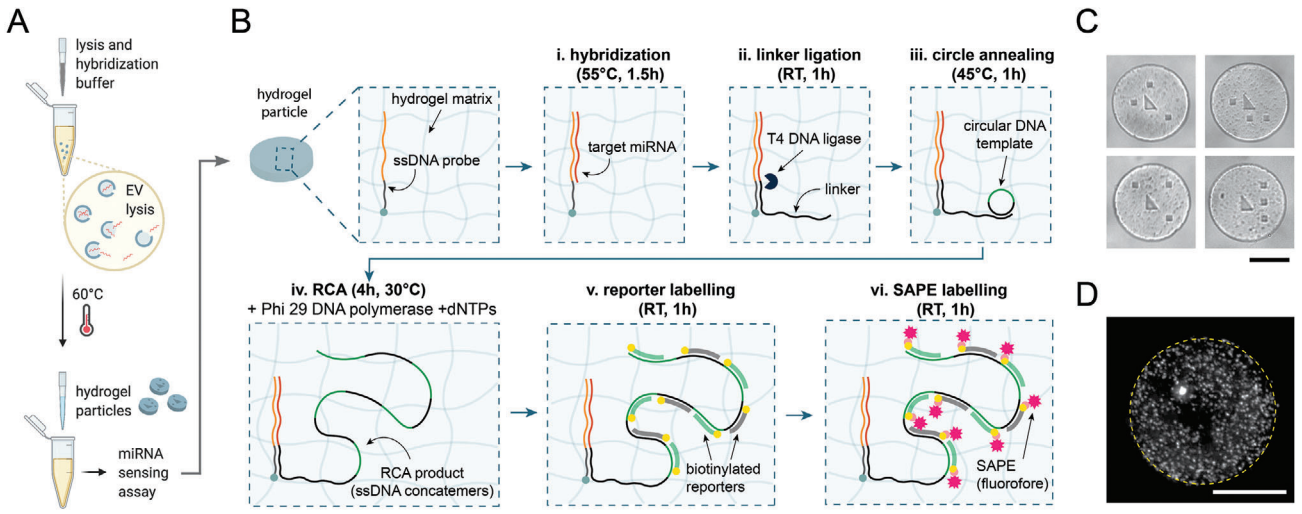

Figure 1. Schematic of EV lysis followed by miRNA capture and detection in encoded hydrogel microparticles. Schematic illustration of A) one-pot lysis and miRNA capture, followed by B) RCA in hydrogel microparticles, involving i) hybridization of the target to the ssDNA probe, ii) ligation of a universal linker, iii) annealing of a circular DNA template, iv) RCA using Phi 29, v) labeling with biotinylated reporters, and vi) labeling with a fluorophore (details can be found in the Experimental Section). C) Microscopy images of four graphically-encoded hydrogel particles with different embedded probes for multiplexed sensing (scale bar = 50 µm). The graphical code, defined by a lithography mask, consists of a triangle surrounded by three squares in different locations. D) Confocal fluorescence microscopy image of a single hydrogel microparticle (with dashed yellow outline) after miRNA detection via RCA showing a speckled pattern with bright spots indicating successful RCA (scale bar = 50 µm).

EV isolation from serum, the assay involves a one-pot EV lysis and miRNA capture step within encoded hydrogel microparticles (**Figure 1**A). To achieve the sensitivity required for quantitative detection, an isothermal amplification strategy is exploited based on rolling circle amplification (RCA) (Figure 1B).[41] The present system offers ease of multiplexing through graphical-encoding of the hydrogel microparticles achieved through synthesis via stop-flow lithography (SFL) techniques previously demonstrated by the group (Figure 1C). The brightfield microscopy images in Figure 1C show the graphical code on four different types of hydrogel microparticles, each functionalized with a ssDNA probe targeting a different miRNA. The graphical code here, defined by the lithography mask used in SFL synthesis of the particles, consists of a triangle surrounded by three squares in different locations. The distinct code, seen in brightfield microscopy, enables us to easily identify the probe within each hydrogel microparticle thus providing a facile and elegant multiplexing strategy. With a fluorescence-based readout and an isothermal amplification strategy, the system offers a large dynamic range (3 orders of magnitude) and a low limit of detection (zeptomole regime), making it amenable for use in diagnostic and prognostic applications (Figure 1D).

2. Results

2.1. EV Isolation and Quantification

There are numerous methods for EV isolation, the most popular being ultracentrifugation, size-exclusion chromatography, or polymeric reagent-based precipitation.[42–44] In this work, polyethylene glycol (PEG)-based precipitation was used as it is faster and more accessible than ultracentrifugation.[45] Based on commercially available formulations and similar recipes in literature,[42,44,46,47] an in-house PEG precipitation recipe was developed using PEG 6000. Briefly, the clarified serum was mixed with 60% w/v PEG 6000 stock solution to a final concentration of 10% w/v PEG 6000. The mixture was thoroughly mixed until it turned cloudy white and then stored upright at 4 °C for 30 min. The mixture was then centrifuged at 10 000 g for 10 min at room temperature, producing a pellet at the bottom of the tube, which was resuspended in filtered phosphate buffered saline (PBS). The PBS resuspension volume was either the same as the starting serum volume (for 1x EV sample) or fourfold less (for 4x EV sample).

All optimization experiments related to EVs were conducted using commercially-purchased human serum from healthy male AB-plasma (Sigma-Aldrich H4522). H4522 is tested under Food and Drug Administration (FDA) requirements and collected under the American Association of Blood Banks (AABB) guidelines. For miRNA dysregulation studies, single-donor lung cancer serum and matched healthy serum (AMSBIO) were used (donors are both females in their 50s). Clinical samples used herein and sourced by AMSBIO, were obtained following official protocols, with appropriate Institutional Review Board/Independent Ethics Committee (IRB/IEC) approval. EV quantification after isolation was performed using nanoparticle tracking analysis (NTA), and microfluidic resistive pulse sensing (Figure S1, Supporting Information), with details discussed in the Experimental Section. Additionally, membrane integrity was assessed with calcein AM stain.[48]

Precipitation based methods for EV isolation offer ease of use, low equipment requirements (only a low-speed centrifuge required), and generally less than 30 min of hands-on time.[49] This allows easier integration into clinical settings as compared to other isolation techniques involving ultracentrifugation or size exclusion chromatography. Nonetheless, there are drawbacks

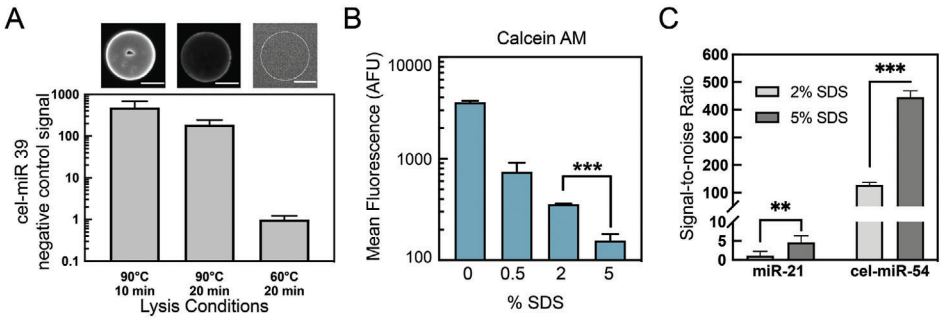

Figure 2. Optimization of Extracellular Vesicle Lysis. A) Effect of lysis temperature on nonspecific signal on negative control *cel*-miR-39 particles. Representative images of negative control particles showing the extent of nonspecific signal. Right-most particle is thresholded to show that no fluorescence is visible. B) Mean Fluorescence from EVs lysed with varying SDS concentration and subsequently incubated with calcein AM dye. *** (p-value<0.001) indicates statistical significance using unpaired t-test ($N = 3$). C) Signal-to-noise ratio (SNR) from serum EVs after lysis with either 2% or 5% SDS (60 °C, 20 min lysis). SNR is calculated as the ratio of the net signal (negative control-subtracted signal) and the standard deviation of the control. In this instance, the control is the signal from the negative control *cel*-miR-39. *cel*-miR-54 represents the positive spike-in control. ** ($p < 0.01$), *** ($p < 0.001$) indicates statistical significance using unpaired t-tests ($N \geq 5$ particles). Error bars throughout represent 1 standard deviation.

such as the high degree of contamination from aggregated proteins, lipoproteins, and the PEG polymer itself.[45] Accordingly, the assay lysis conditions were optimized to avoid fouling from these contaminants that coprecipitate with the EVs.

2.2. EV Lysis

PEG hydrogel microparticles have been shown to be nonfouling and compatible with a variety of complex samples like serum, cell lysate, and FFPE tissue sections, using a one-pot lysis and miRNA hybridization protocol.[35–37] The serum lysis protocol, in which the serum was combined with lysis buffer, containing sodium dodecyl sulfate (SDS), and then heated to 90 °C for 10 min before addition of particles resulted in very high levels of nonspecific signal when used with 4x concentrated EVs (**Figure 2**A). Increasing the time for this preheat step to 20 min lowered the nonspecific signal only marginally. However, by reducing the temperature to 60 °C, this nonspecific signal was eliminated as shown in Figure 2A. It is hypothesized that the high nonspecific signal at 90 °C was caused by lipids and lipoproteins aggregating and sticking to the particles during hybridization, causing streptavidin-r-phycoerythrin (SAPE) to nonspecifically adsorb to the particles during the labeling step. The lipid and lipoprotein contents are highly dependent on the donor of the serum, as well as the blood collection protocol.[50] To ensure that the protocol would be valid for any type of serum sample, regardless of lipid content, a 60 °C preheat step for 20 min was chosen for EV lysis.

Additionally, the SDS concentration for EV lysis was optimized to maximize exosome rupture without inhibiting miRNA hybridization using calcein AM dye as an indicator for intact membranes.[48] Compared to previous work with cells in which 2% SDS was used,[36] EVs have greater membrane surface area at the concentrations used for these assays. Calcein AM dye is nonfluorescent until it is cleaved into a fluorescent product by esterases present in intact EVs. As the EVs are lysed, the esterases are denatured due to the proteinase K and thus no fluorescent product accumulates within the sample.[48] The results in Figure 2B show a clear decrease in fluorescence with increasing SDS concentration.

MiRNA hybridization efficiency was also assessed at both 2% and 5% SDS to ensure that the higher SDS concentration did not interfere with hybridization. A standard (nonamplified) assay was conducted with 4x EVs with particles containing probes for miR-21, *cel*-miR-54 (spiked-in positive control), and *cel*-miR-39 (negative control). Figure 2C shows the signal-to-noise ratio (SNR) for miR-21, and *cel*-miR-54. While the net signals (negative control-subtracted signal) are similar for both SDS concentrations, the noise (standard deviation of the negative control signal) is lower at 5% SDS, resulting in a higher SNR for 5% SDS. Signal from *cel*-miR-54 target spiked into both EVs or neat buffer (PBS) is similar, demonstrating that the complex matrix present in an EV sample does not hamper miRNA capture specificity (Figure S3, Supporting Information).

Based on these sets of experiments, an optimized lysis protocol was developed, which consisted of heating the EV sample at 60 °C for 20 min in 5% SDS, 350×10^{-3} M NaCl in Tris-EDTA buffer with 0.05% Tween-20 (TET), followed by the addition of particles, proteinase K (16 U mL^{-1}) and positive control target to start miRNA hybridization.

2.3. Optimizing RCA for EV-miRNA Detection

In order to achieve the sensitivity required for EV-miRNA detection from biological samples, RCA was introduced to the standard miRNA detection assay. This isothermal amplification strategy can improve sensitivity without adding complexity as it requires a single temperature of 30 °C.[41] Also, RCA amplifies the signal without modifying the number of target molecules, thus avoiding biases common in PCR-based assays. Briefly, RCA involves the replication of a circular template DNA (circDNA) with a polymerase enzyme (Phi29 DNA polymerase) (Figure 1B).[51] This generates long single-stranded concatemers of DNA which can be labeled and detected in a variety of ways, herein, by labeling with biotinylated oligomers then tagging with a fluorescent reporter (SAPE). Thus, for each target molecule, multiple

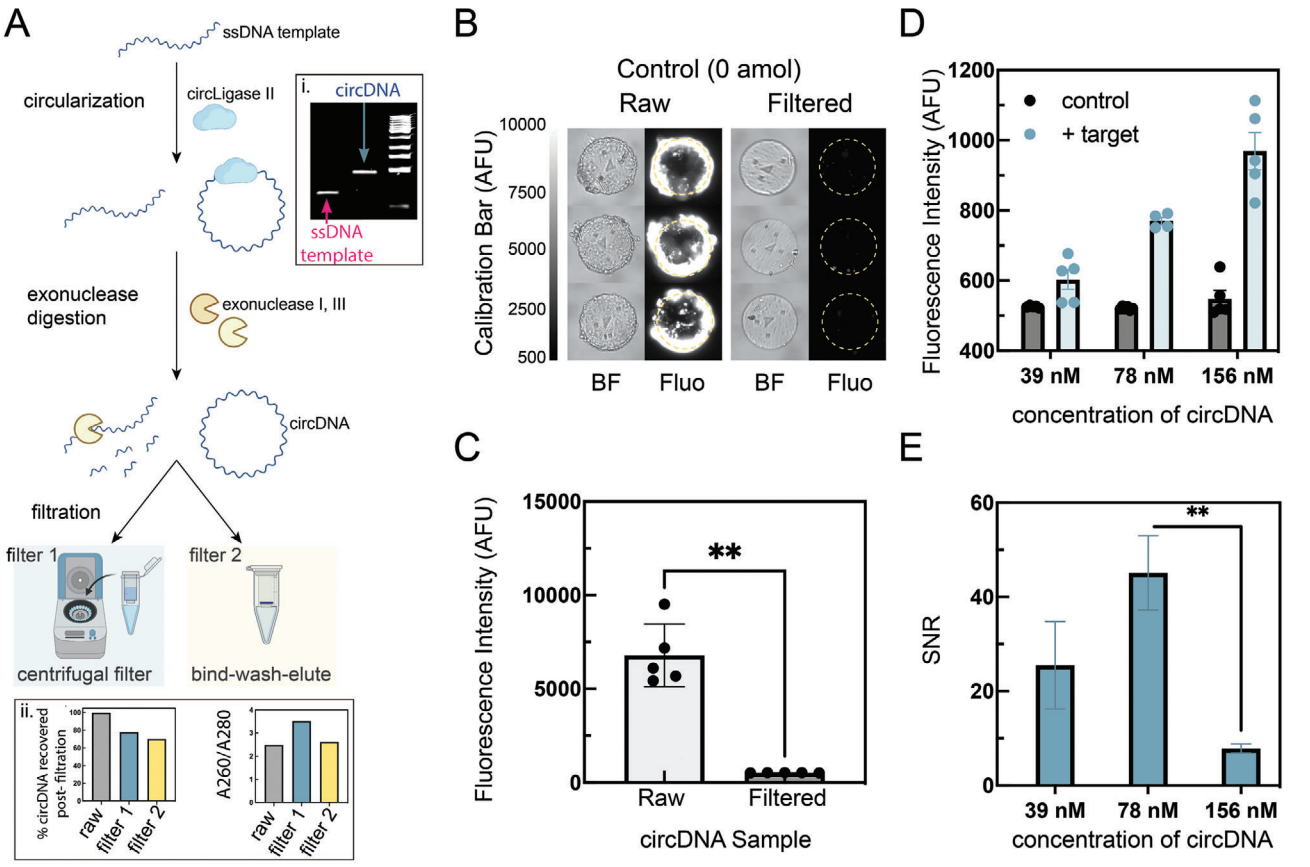

Figure 3. Optimization of RCA-based assay for EV-miRNA detection. A) Synthesis and filtration of circDNA from precursor ssDNA template, showing i) gel electrophoresis indicating successful circularization (Figure S2, Supporting Information), and ii) Nanodrop analysis showing greater % circDNA recovery and higher A260/A280 ratio for filter 1. B) Brightfield (BF) and fluorescence (FL) microscopy images of control particles (0 amol target miRNA) after the assay using raw (unfiltered) circDNA versus filtered circDNA (filter 1) showing high background nonspecific fluorescence using raw circDNA. C) Fluorescence intensity of control particles after the assay using the raw versus filtered (filter 1) circDNA. ** indicates statistical significance using unpaired *t*-test (p-value < 0.01) ($N = 5$). D) Fluorescence intensity of the hydrogel particles without (control) and with target miRNA (+target) using varying concentrations of circDNA in the assay ($N = 5$). E) Signal-to-noise (SNR) ratios of the RCA assay using different concentrations of circDNA. SNR is calculated as the ratio of the net signal (control-subtracted signal) and the standard deviation of the negative control. In this instance, the control is the signal from the 0 amol condition (i.e., no target miRNA). Error bars throughout show standard error of mean. ** indicates significance using one-way ANOVA: 78×10^{-9} M versus 156×10^{-9} M, $p < 0.01$ ($N = 5$).

fluorophores could be tagged, amplifying the signal generated from even low concentrations of miRNA. As outlined in Figure 1B, RCA-based sensing involved i) miRNA hybridization to the hydrogel-functionalized ssDNA probe, followed by ii) ligation of a universal linker complementary to the circular template. After iii) annealing of the circDNA template, iv) RCA amplification was conducted for 4 h (30 °C) by adding Phi29 polymerase and dNTPs, generating long ssDNA concatemers. v) These were labeled by two biotinylated reporters, followed by vi) tagging with SAPE. Further details for the RCA Assay protocol can be found in the Experimental Section under the heading "RCA miRNA Assay Protocol." Our previous work has demonstrated that the PEG-based hydrogel matrix used herein is compatible with RCA, but the technique's compatibility with biological samples was limited by low reliability and limited sensitivity due to high nonspecific fluorescent signals (i.e., background noise).[35]

To improve the efficiency of RCA (i.e., increase signal-to-noise ratios), two strategies were implemented: i) purification of the circDNA template postsynthesis, and ii) optimizing the concentration of circDNA. First, circDNA was synthesized based on a published protocol.[52] Briefly, 50 nt precursor template DNA was circularized using CircLigase II (Epicentre Biotechnologies) followed by enzymatic deactivation and exonuclease digestion to remove any remaining linear DNA (**Figure 3**A). Confirmation of circularization was visualized by gel electrophoresis (15% Mini-PROTEAN TBE-Urea gel) and analyzed by comparing the synthesized circular template and its linear precursor DNA bands (Figure 3A,I; and Figure S2, Supporting Information). Next, to reduce nonspecific signals, we sought to filter the circDNA solution and remove the enzymes which may interfere with subsequent RCA steps and thus contribute to the nonspecific signals. Two different filtration strategies were investigated: 1) centrifugal filtration using a 30 kDa MWCO filter (Amicon Ultra-0.5 mL Centrifugal Filters) and 2) a bind-wash-elute strategy using a Monarch DNA Cleanup Column (New England Biolabs (NEB) T1034L). Nanodrop spectrophotometric analysis was performed on the raw

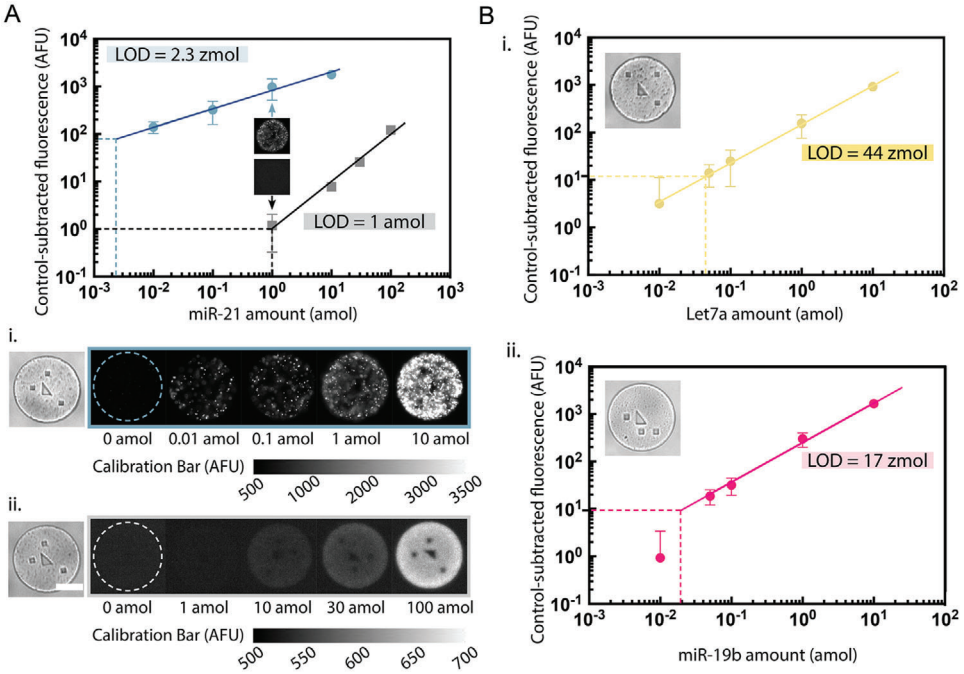

Figure 4. Comparing sensitivity and dynamic range of RCA-based assay versus the standard assay. A) Calibration curve with standard (black) and RCA (blue) assay with varying amounts of synthetic miR-21 target ($N \geq 7$ particles per concentration). Dashed lines indicate LOD as three times standard deviation of control (0 amol) condition. Representative particles after miRNA detection with the RCA i) and standard ii) assay (scale bar = 50 µm). B) Calibration curves and corresponding LOD for let-7a i) and miR-19b ii). Error bars throughout represent standard deviation ($N \geq 6$ particles per concentration).

(unfiltered) circDNA solution in addition to the filtered solution with both techniques in order to quantify circDNA concentration and assess sample purity. Centrifugal filtration (filter 1) was chosen for all further experiments as it provided higher percentage recovery of circDNA (78%) and higher purity (A260/A280 of 3.5) when compared to filter (2), with 70% recovery and A260/A280 of 2.6 (Figure 3A, ii).

Next, to compare the nonspecific signals generated using the raw and filtered circDNA, RCA was performed in the presence of no target miRNA (i.e., 0 amol miRNA). Ideally, very low or no fluorescence should be detectable in the hydrogel particles. As seen in Figure 3B, brightfield (BF) microscopy images of the raw circDNA sample had a textured surface with contaminants around the edge. In contrast, clean particles with a smooth surface were observed in the BF images of the filtered circDNA samples. The corresponding fluorescence microscopy images also showed a highly fluorescent rim surrounding each particle using the raw circDNA, while no fluorescence was apparent using the filtered circDNA. By quantifying these fluorescent signals (ImageJ, NIH), a statistically significant reduction in nonspecific fluorescence could be achieved by filtering the circDNA prior to use in RCA (unpaired *t*-test, $p < 0.01$) (Figure 3C).

The second strategy used to improve RCA efficiency involved optimizing the concentration of filtered circDNA used in RCA. For this, three different concentrations of filtered circDNA were evaluated in the circDNA annealing step: i) standard 39×10^{-9} M, (ii) double the standard at 78 nm, and iii) four times the standard at 156×10^{-9} M of circDNA in the final particle solution. For each circDNA concentration, the fluorescence intensity of the hydrogel particles in the presence of 1 amol target miRNA was compared to that in the absence of target (i.e., control) (Figure 3D). The highest SNR was observed for the 78×10^{-9} M condition (one-way ANOVA: 78×10^{-9} M vs 156×10^{-9} M, $p < 0.01$); thus, this condition was used for all further experiments (Figure 3E).

2.4. Sensitivity and Dynamic Range of RCA-Based Assay: Calibration Curves

After optimizing the performance of the RCA-based assay, its sensitivity and dynamic range were characterized and compared to that of the standard assay. **Figure 4**A shows calibration curves for both the standard and RCA-based assays, conducted by varying the amount of synthetic target miR-21. A standard hybridization buffer (no SDS, or proteinase K) was used for synthetic target assays. Compared to the standard assay with a limit of detection (LOD) of 1 amol, the enhanced RCA strategy offered an LOD of 2.3 zmol, representing three orders of magnitude improvement in sensitivity. This also represents an improvement in sensitivity over previous iterations of RCA in hydrogel particles by ~sixfold, and a considerable improvement over other multiplexed amplification techniques, such as hybridization chain reaction.[53–55] Another advantage of the RCA-based assay is its large dynamic range, from low zeptomoles to tens of attomoles, spanning over three orders of magnitude. Compared to other isothermal amplification-based strategies, this assay demonstrates greater sensitivity and multiplexing capability, as well as the amenability with real biological samples (Table S2,

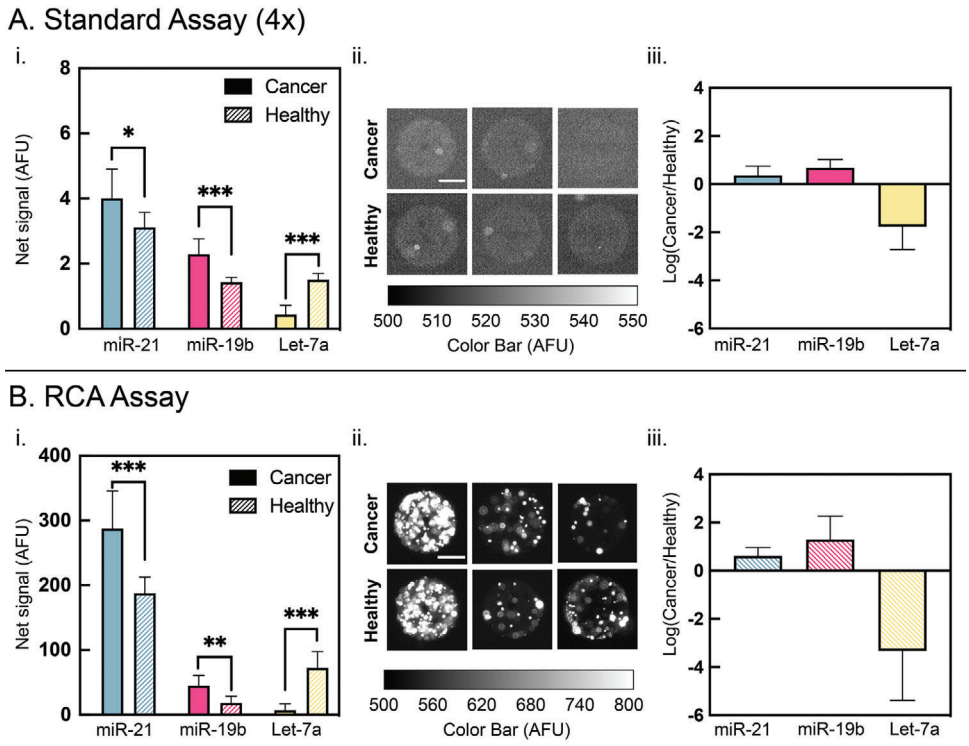

Figure 5. Comparing the efficiency of multiplex EV-miRNA detection from serum samples using the standard assay A) versus the RCA assay B), noting importantly that 4x concentrated EVs were used for the standard assay, whereas 1x concentrated EVs were used for the RCA assay. i) Net signal after multiplex detection of three endogenous miRNAs from the lung cancer patient sample (solid bars) versus the healthy patient sample (hashed bars). ii) Representative particles after miRNA detection with the two sensing assays. iii) Fold change in signal between cancer and healthy EVs. ** ($p < 0.01$), *** ($p < 0.001$) indicates statistical significance using unpaired *t*-tests ($N \geq 5$ particles). Error bars throughout represent 1 standard deviation. Scale bar shows 50 µm.

Supporting Information). Indeed, it offers comparable sensitivities to the gold-standard strategies for miRNA detection while eliminating the need for thermal cycling, expensive equipment and trained personnel.

Calibration curves for two other miRNA biomarkers, let-7a and miR-19b, were also conducted and the LODs calculated and recorded as shown in Figure 4B. The three miRNAs (miR-21, let-7a, and miR-19b) were chosen in this work as they have been shown in the literature to be dysregulated in the sera of lung cancer patients when compared to healthy controls, thus representing promising disease biomarkers.[9,56,57]

2.5. EV-miRNA Detection from Biological Samples

To demonstrate the ability of hydrogel particle-based detection of EV-miRNA, we sought to profile the miRNA dysregulation patterns from EVs isolated from a lung cancer patient serum and matched healthy control serum. Using the optimized lysis protocol and standard miRNA detection assay with 4x concentrated Evs, only miR-21, and miR-19b were detectable from both lung cancer and matched healthy patient EVs (**Figure 5**A). let-7a was only detectable in healthy EVs. Moreover, all these targets are just below the limit of detection (SNR = 3) for the standard assay, and well below the limit of quantification (SNR = 10). To achieve the sensitivity necessary to reliably detect miRNA from 1x concentrated EVs, RCA was coupled with the lysis and hybridization protocol for EV-miRNA detection.

With higher sensitivity afforded by RCA, we were able to detect all three miRNA (miR-21, miR-19b, let-7a) from 1x concentration EVs as shown in Figure 5B. The miRNA profiles between the two assays are similar and show a distinct dysregulation pattern in line with literature in which both miR-21 and miR-19b are upregulated in cancer, while let-7a is downregulated and acts as a tumor suppressor.[56,57] Moreover, the similarity in miRNA dysregulation profiles between the standard assay and RCA demonstrates that RCA as an amplification strategy does not introduce biases common with other amplification strategies such as RT-PCR.[23,40] Due to their short length, miRNA detection using PCR-based assays could introduce bias through, for example, preferential amplification based on the miRNA G/C content.[58]

In this work, by combining absolute miRNA quantitation using the hydrogel particle platform and RCA, in conjugation with EV concentration data, we can calculate average miRNA copies per EV particle as shown in **Table 1**. Moreover, the bias and loss associated with RNA extraction is avoided completely with the direct lysis and capture protocol.[59]

The literature on absolute miRNA quantification, particularly in exosomes and EVs is limited. However, one study by Chevillet et al. used ddPCR to profile the most abundant miRNA

Table 1. Summary of average EV concentrations and miRNA copies for lung cancer and match healthy serum EVs. Values reported as mean +/− SEM.

miRNA	Average EV-miRNA copies [μL Serum][a]		Average EV-miRNA copies [EV][b]	
	Cancer EV	Healthy EV	Cancer EV	Healthy EV
Hsa-miR-21	1900 ± 600	640 ± 170	$11 \pm 3.1 \times 10^{-8}$	$1.4 \pm 0.4 \times 10^{-8}$
Hsa-miR-19b	2900 ± 400	1100 ± 200	$16 \pm 2.3 \times 10^{-8}$	$2.3 \pm 0.5 \times 10^{-8}$
Hsa-let-7a	1300 ± 300	10000 ± 2000	$7.2 \pm 1.5 \times 10^{-8}$	$22 \pm 4 \times 10^{-8}$

[a] miRNA copy numbers were calculated from net signals from fluorescence measurements using calibration curves for the respective miRNA [b] EV concentrations used are average MRPS measurements (75–150 nm diameter size range) for the lung cancer and healthy control EVs.

from a range of samples including healthy and cancer patient plasma.[22] For these most abundant miRNAs, the copy numbers ranged from $5 \times 10^4 - 2 \times 10^6$ miRNA copies μL^{-1} plasma, and copies/EV values ranged from $\approx 10^{-5} - 10^{-3}$. Moreover, they showed that there is considerable human-to-human variation in both EV counts and miRNA copy numbers.[22] Another study into the EV-miRNA profiles in control and melanoma cancer plasma found miRNA concentrations of $\approx 9.8 \times 10^3$copies μL^{-1} plasma, for miR-19b and $\approx 1.4 \times 10^4$ copies μ^{-1}L plasma for miR-21 in their control cohort (n = 13 patients) based on RT-PCR with a known spiked-in synthetic target for normalization.[60] Finally, two non-PCR based detection methods found single fM concentrations for exosomal miR-10b in healthy normal donor plasma, as measured by localized surface plasmon resonance (LSPR) and surface enhanced Raman spectroscopy (SERS), which would correspond to $\approx 1 \times 10^3$ copies μL^{-1} plasma.[61,62] Plasma and serum are known to have similar miRNA concentrations, and hence the plasma-based studies are reasonable comparisons for serum EV-miRNA concentrations.[12]

Given the differences in exosome isolation methods and miRNA detection methods, the copies numbers and copies/EV values calculated using our hydrogel platform agree with the few other absolute measurements of EV-derived miRNA concentrations in literature, particularly from blood serum or plasma. The data also agree with the general trend of the low stoichiometry and low abundance of EV-associated miRNAs in plasma and serum.[22]

3. Conclusion

In this study, we presented a facile and highly sensitive platform for multiplexed detection of EV-associated miRNA down to zeptomole amounts, and showed how this platform can be used to determine EV-miRNA dysregulation patterns in human samples, namely serum from a pair of lung cancer and matched healthy patients. EV lysis was optimized for direct detection of miRNAs from isolated EVs using a one-pot lysis and miRNA hybridization recipe. Further, an isothermal signal amplification strategy, based on rolling circle amplification, was utilized for ultrasensitive measurements of the EV-associated miRNA. This resulted in absolute quantification, providing miRNA copy number estimates per EV and per microliter in agreement with other studies in literature. Importantly, the optimized RCA-based assay was able to quantify EV-miRNA biomarkers isolated from serum without the need for sample preconcentration or RNA extraction, which paves the way for quantitative measurements from a variety of samples expected to have low-abundance of miRNA and encourages further research into EV-miRNA biomarkers for non-invasive cancer diagnosis and monitoring.

4. Experimental Section

PEG-Based EV Isolation: EVs were isolated from the sera of lung cancer and healthy matched subjects by polyethylene glycol precipitation. Serum aliquots were thawed in a water bath at room temperature and then centrifuged at 2000xg for 30 min to clarify the serum and remove debris. EVs were isolated using a modified PEG precipitation recipe. This PEG precipitation recipe was based on PEG 6000 based on both commercially available formulations and similar recipes in literature.[42,44,46,47] A 60% w/v PEG 6000 solution was made by dissolving PEG 6000 in nuclease-free water and stirring on a hot plate at 60 °C until the solution was clear and uniform. This solution was stored at 4 °C. The PEG solution was added to the clarified serum in a 5:1 ratio resulting in a final concentration of 10% w/v PEG 6000. The mixture was thoroughly pipette mixed until it turned cloudy white and then stored upright at 4 °C for 30 min. The mixture was then centrifuged at 10 000xg for 10 min at room temperature. The supernatant was carefully removed without disturbing the pellet using a pipette tip. The pellet was resuspended in 20 nm filtered PBS (PBS filtered through a 20 nm Anotop syringe filter (Whatman)) by gentle mixing on a thermoshaker at room temperature for 30 min. The PBS volume was either the same as the starting serum volume (1x EV concentration) or fourfold less (4x EV concentration). The purified EVs were split into aliquots and stored at 4 °C for up to 48 h, and then stored at −20 °C for medium term storage (1 week to 2 months). For long term storage, EV and serum aliquots were moved to −80 °C.

Nanoparticle Tracking Analysis (NTA): NTA was performed on the Malvern Nanosight LM10 instrument. EVs isolated from serum were diluted 10 000x in 20 nm filtered PBS and introduced to the measurement chamber via a syringe pump. 31 videos, 30 s each were taken of the particle scatter, with a 5 s flush (at 150 μL min^{-1}) in between to introduce new particles into the field of view. A MATLAB script controlled the syringe pump to coordinate with the timing of video acquisition. The detected number of particles in a field of view determined the absolute concentration measured by the Nanosight, while the particles with completed tracks informed the size distribution.

Microfluidic Resistive Pulse Sensing (MRPS): MRPS was conducted using the Spectradyne nCS1, using both the C-300 (size range 50–300 nm) and C-400 cartridges (size range 65–400 nm). EVs isolated from serum were diluted 200x-1000x in 20 nm filtered PBS with 2% tween-20 and a 5 μL sample was added to the cartridge and inserted into the instrument according to manufacturer protocols. At least 1000 particle events were collected for the size range of interest. The data were filtered according to user-defined thresholds and filters such that only events with diameters >75 nm, S/N >25, and transit time < 80 ms were included for analysis. These filters were set based on calibration runs of NIST-certified calibration beads (93 nm diameter).

PDMS Microfluidic Device Fabrication: Microfluidic channels for particle synthesis were fabricated in polydimethylsiloxane (PDMS) using previously published methods. PDMS (Sylgard 184, Dow Corning) was mixed in a 10:1 base: crosslinker ratio and poured over a SU-8 photoresist mold, fabricated using standard photolithography techniques. PDMS mixing was done by hand using a glass stir rod for about 1 min. After pouring the PDMS over the mold, the PDMS was degassed under vacuum for 2 × 1 min intervals using a desiccator. The PDMS was allowed to sit at room temperature for at least another 20 min until all the bubbles had disappeared, before placing in a 65 °C oven to cure overnight. The PDMS channels were cut using a clean scalpel and then cleaned by sonicating in ethanol. Inlets and outlets were punched using a biopsy punch (1.5 mm

inlet, 4 mm outlet). The PDMS channels were placed on a glass coverslip coated in half-cured PDMS (10:1 ratio, cured for 25–30 min at 65 °C). The resulting device was baked overnight at 65 °C to complete the bonding process.

Hydrogel Particle Synthesis: Graphically encoded hydrogel microparticles containing target-specific ssDNA probes were fabricated in 42 µm tall polydimethylsiloxane (PDMS, Sylgard 184, Dow Corning) microfluidic channels via stop-flow lithography (SFL) techniques as described in previously published methods.[39] Particles were made from a PEG-based solution containing 20% v/v poly(ethylene glycol) diacrylate 700, 40% v/v poly(ethylene glycol) 600, 5% v/v Darocur 1173 photoinitiator (Sigma-Aldrich), and 35% 3x Tris-EDTA (TE) buffer (pH 8.0), copolymerized with acrydite-modified ssDNA capture probes (Integrated DNA Technologies, IDT). Photolithography masks placed in the field-stop of the microscope determined the shape of the code on each particle, thus enabling multiplexing using a single fluorescent dye. Particles were made in a circular disk shape with a nominal diameter of 100 µm with a graphical code in the center. In this design, the graphical code consisted of a triangle surrounded by three squares in different locations. A different code is used for each miRNA target, enabling multiplexing with a facile strategy. Particles are collected from the outlet and washed twice with TET (1xTE buffer with 0.05% Tween-20). Each wash consists of adding 400 µL of buffer to the microfuge tube containing the particles, vortexing briefly, centrifuging for 45 s to sediment the particles, and removing 400 µL of supernatant. Particles were then oxidized by incubating them for 5 min with 500×10^{-6} M $KMnO_4$ in 0.1 M Tris-HCl pH 8.8. Particles were washed 3x in TET and stored in TET at 4 °C. By controlling the UV light exposure, flow conditions, prepolymer composition, and microfluidic channel dimensions during stop-flow lithography, high reproducibility in particle size (mean diameter = 107.9 µm, CV = 1.3%, Figure S4, Supporting Information), physicochemical morphology and DNA probe loading (≈11% incorporation) is achieved. Particles made with PEG 600 as the porogen, have been shown to have high enough porosity to allow for the diffusion and capture of mRNA (R_g ≈10 nm).[63]

EV Lysis Optimization: Varying concentrations of SDS (0.5–5%) were assessed for performance and compatibility with miRNA hybridization. Lysis performance was assessed using Calcein AM, as an indicator for intact membranes. The dye molecule is nonfluorescent until it enters the EVs and is cleaved by esterases into a fluorescent product.[48] Isolated EVs from Sigma-Aldrich serum were combined with lysis buffer containing various SDS concentrations for 20 min at 60 °C. Calcein AM dye was added at a 1:100 dilution of the stock solution, to a final concentration of 10×10^{-6} M and incubated for 20 min at 37 °C to promote esterase activity. The fluorescence was measured in a Tecan F200 Plate Reader with an excitation of 485 nm and emission of 515 nm in a black-walled 96-well plate.

For optimization using the standard miRNA assay, the hybridization buffer was modified with added SDS (2–5%). The EV sample was preheated for either 60 or 90 °C for varying amounts of time in the modified lysis and hybridization buffer. After lysis, 1 µL of Proteinase K (final concentration 16 U mL^{-1}) was added to each tube along with particles containing probes for miR-21, *cel*-miR-54 (positive control), and *cel*-miR-39 (negative control). Finally, 100 amol synthetic *cel*-miR-54 target was spiked into each tube.

Standard miRNA Assay Protocol: Detection involved miRNA hybridization, ligation of a universal biotinylated linker, then labeling with SAPE. 25 µL of purified EVs (4x concentration) were combined with 5 µL of 3.75 M NaCl and 10 µL of 25% w/v SDS. Both the NaCl and SDS solutions were made in 1x TE buffer with 0.125% Tween-20. EV lysis was conducted for 20 min at 60 °C. After lysis, 1 µL of Proteinase K (stock at 800 U mL^{-1}, NEB) was added to each tube along with particles containing miRNA-specific probes were added to the reaction (≈25 particles per miRNA target per reaction), and 100 amol positive control target spike-in, *cel*-mir-54. The final lysis-hybridization buffer composition was 5% SDS, 16 U mL^{-1} Proteinase K, 350×10^{-3} M NaCl, and 0.05% Tween-20 in 1xTE in a 50 µL reaction volume.

Hybridization was conducted at 55 °C for 90 min, after which particles were washed 3 times in rinse buffer (TET + 50×10^{-3} M NaCl). Each wash step consisted of adding 400 µL rinse buffer to 50 µL of particle solution, followed by a brief vortex and then centrifuging for 1 min and removing 400 µL of supernatant. A universal biotinylated adapter sequence was then ligated onto each captured miRNA target in a 30 min ligation step at 21.5 °C using T4 DNA Ligase (NEB). The particles were washed 3 times before labeling with 2 µg mL^{-1} streptavidin R-phycoerythrin (SAPE, Thermofisher) for 45 min at 21.5 °C. All particle incubation steps were conducted on a thermoshaker (Benchmark) with shaking at 1500 rpm. Particles were washed 3 times and then imaged on a glass coverslip using a fluorescence microscope (Zeiss Axio Observer) equipped with a LED excitation source (X-Cite 120 LED) and appropriate filter set for phycoerythrin (Semrock ex = 520/60, em = 607/70). Images were captured using a CCD camera (Andor Clara) and analyzed with ImageJ.

CircDNA Synthesis, Validation, and Filtration: Based on a protocol by Schopf et al. (2010),[52] the circular template was prepared from a 50 nt linear precursor DNA using a CircLigase II enzyme (Epicentre Biotechnologies) followed by enzymatic deactivation and exonuclease digestion to remove any remaining linear DNA. Confirmation of circularization was visualized by gel electrophoresis (15% Mini-PROTEAN TBE-Urea gel) and analyzed by comparing the synthesized circular template and its linear precursor DNA bands. Next, prepared circDNA solution was purified following two different strategies: i) centrifugal filtration or ii) spin-wash-elute technique. For i), the circDNA solution was passed through a centrifugal filter (Amicon Ultra-0.5 mL, MWCO 30 kDa) at 14000 g (30 min) at RT. The flow-through was collected as filtered circDNA and analyzed via Nanodrop. For ii), the circDNA solution was loaded into a binding column (NEB, T1020), then washed twice with 200 µL DNA Wash Buffer and spun for 1 min at 16000 x g. The column was then carefully transferred to a clean 1.5 mL microfuge tube for elution. 23 µL of DNA Elution Buffer was to the center of the matrix, and after a 1 min wait spun at 16000 x g for 1 min to elute the circDNA. The purity of circDNA after filtration with filter i) and filter ii) was analyzed via Nanodrop (NanoDrop 2000/2000c Spectrophotometer). CircDNA with filter i) gave a higher A260/A280 ratio of 3.51 and greater concentration of 142.8 ng μL^{-1} when compared to filter ii) which gave an A260/A280 ratio of 2.62 and concentration of 128.1 ng μL^{-1}.

RCA miRNA Assay Protocol: 25 µL of purified EVs (1x concentration) was combined with 5 µL of 3.75 M NaCl and 10 µL of 25% w/v SDS. Both the NaCl and SDS solutions were made in 1x TE buffer with 0.125% Tween-20. EV lysis was conducted for 20 min at 60 °C. After lysis, 1 µL of Proteinase K (stock at 800 U mL^{-1}, NEB) was added to each tube along with particles containing miRNA-specific probes were added to the reaction (≈25 particles per miRNA target per reaction), and 1 amol positive control target spike-in, *cel*-mir-54. The final lysis-hybridization buffer composition was 5% SDS, 16 U mL^{-1} Proteinase K, 350×10^{-3} M NaCl, and 0.05% Tween-20 in 1xTE in a 50 µL reaction volume.

RCA-based sensing involved miRNA hybridization followed by ligation of a linker complementary to the circular template. After template annealing, amplification was conducted for 4 h (30 °C) by adding Phi29 polymerase and dNTPs, generating long ssDNA concatemers. These were labeled by two biotinylated reporters, followed by tagging with SAPE. Hybridization was conducted at 55 °C for 90 min in a thermomixer (1500 rpm), after which particles were washed 3 times in rinse buffer (TET with 50×10^{-3} M NaCl). Each wash step consisted of adding 400 µL rinse buffer to 50 µL of particle solution, followed by a brief vortex and then centrifuging for 1 min and removing 400 µL of supernatant. A linker sequence (complementary to the circDNA) was then ligated onto each captured miRNA target in a 1 h ligation step at 21.5 °C using T4 DNA Ligase (NEB). The particles were washed 3 times with rinse buffer. Next, to anneal the circDNA to the linker, 1.2 µL (unless otherwise noted) of filtered circDNA was pipetted into the particle solution and incubated at 45 °C for 1 h. After three washes in rinse buffer and a final wash in TET, an RCA buffer mix was prepared as outlined in **Table 2** below. 200 µL of the buffer mix was added to the 50 µL particle solution and incubated for 4 h at 30 °C. After 3 washes in rinse buffer, two biotinylated reporters (complementary to the ssDNA RCA product) were added to the particle solution to a final concentration of 10×10^{-6} M in rinse buffer, and incubated at RT for 1 h. Finally, after three washes in rinse buffer, labeling was conducted with 2 µg mL^{-1} SAPE for 45 min at 21.5 °C. All particle incubation steps were conducted on a thermoshaker (Benchmark) with shaking

Table 2. RCA buffer components and reaction concentrations.

Component	Stock concentration	Volume added [µL]	Reaction tube concentration
NEB2	10x	25	1x
Bovine Serum Albumin	20 mg mL^{-1}	2.5	200 µg mL^{-1}
1,4-Dithiothreitol (DTT)	1 M	1.25	5×10^{-3} M
dNTPs	10×10^{-3} M	3.75	150×10^{-6} M (each)
TET	1x	157.5	<1x
Phi29	10 000 U mL^{-1}	10	400 U mL^{-1}

at 1500 rpm. See Table S1 (Supporting Information) for all nucleic acid sequences.

Particles were washed 3 times and then imaged following the same procedure as the standard assay protocol.

For absolute miRNA copy number estimates, the average net signals for each miRNA in each sample were converted to miRNA attomole amounts using the respective miRNA calibration curves. These attomole amounts were then converted to copy number μL^{-1} serum or copy number/ EV, using average EV concentration measurements from MRPS. Standard errors for average copy numbers were determined using Monte Carlo simulation of the inverse calibration curve equation using the standard deviations of the net signal measurements and standard errors in calibration curve coefficients.

Statistical Analysis: Details of the statistical analysis are outlined in the appropriate sections and figure captions. Data are presented as mean ± standard deviation or standard error of mean (as indicated in the figure captions). Net signal is calculated as the negative control-subtracted signal. Noise is calculated as the standard deviation of the negative control signal. Signal-to-noise ratio is calculated as the ratio of the net signal to the noise. Statistical analysis involved conducting two-tailed, unpaired *t*-tests, or one-way ANOVA, with significance defined by p-values < 0.05 as indicated in the figure captions. Sample sizes used in each statistical comparison are indicated in the figure captions. Monte Carlo simulations to determine standard error of mean of average copy numbers were determined using @Risk Add-in within Microsoft Excel. Unless otherwise noted, statistical analysis testing was conducted using Microsoft Excel or Graphpad Prism (v 9.1.0).

Supporting Information

Supporting Information is available from the Wiley Online Library or from the author.

Acknowledgements

The authors gratefully acknowledge funding from the National Institutes of Health (NIH) R01 grant (No. 1R01CA235740-01A1) and the Natural Sciences & Engineering Research Council (NSERC) of Canada. This work was supported in part by the Koch Institute Support (core) Grant No. P30-CA14051 from the National Cancer Institute. They thank the Koch Institute's Robert A. Swanson (1969) Biotechnology Center for technical support, specifically the nanotechnology materials core.

Conflict of Interest

The authors declare no conflict of interest.

Data Availability Statement

The data that support the findings of this study are available in the supplementary material of this article.

Keywords

biomarkers, cancer, extracellular vesicles, hydrogels, liquid biopsies, microRNA

Received: October 27, 2021
Revised: January 6, 2022
Published online: January 22, 2022

[1] V. Ambros, *Nature* **2004**, *431*, 350.
[2] D. P. Bartel, *Cell* **2004**, *116*, 281.
[3] J. Lu, G. Getz, E. A. Miska, E. Alvarez-Saavedra, J. Lamb, D. Peck, A. Sweet-Cordero, B. L. Ebert, R. H. Mak, A. A. Ferrando, J. R. Downing, T. Jacks, H. R. Horvitz, T. R. Golub, *Nature* **2005**, *435*, 834.
[4] P. Ulivi, W. Zoli, *Molecules* **2014**, *19*, 8220.
[5] A. R. Halvorsen, Å. Helland, P. Gromov, V. T. Wielenga, M. L. M. Talman, N. Brunner, V. Sandhu, A. L. Børresen-Dale, I. Gromova, V. D. Haakensen, *Mol. Oncol.* **2017**, *11*, 220.
[6] S. Volinia, M. Galasso, M. E. Sana, T. F. Wise, J. Palatini, K. Huebner, C. M. Croce, *Proc. Natl. Acad. Sci. USA* **2012**, *109*, 3024.
[7] C. C. Pritchard, H. H. Cheng, M. Tewari, *Nat. Rev. Genet.* **2012**, *13*, 358.
[8] S. Anfossi, A. Babayan, K. Pantel, G. A. Calin, *Nat. Rev. Clin. Oncol.* **2018**, *15*, 541.
[9] G. A. Calin, C. M. Croce, *Nat. Rev. Cancer* **2006**, *6*, 857.
[10] C. Mall, D. M. Rocke, B. Durbin-Johnson, R. H. Weiss, *Biomark Med.* **2013**, *7*, 623.
[11] C. Glinge, S. Clauss, K. Boddum, R. Jabbari, J. Jabbari, B. Risgaard, P. Tomsits, B. Hildebrand, S. Kääb, R. Wakili, T. Jespersen, J. Tfelt-Hansen, *PLoS One* **2017**, *12*, e0167969.
[12] P. S. Mitchell, R. K. Parkin, E. M. Kroh, B. R. Fritz, S. K. Wyman, E. L. Pogosova-Agadjanyan, A. Peterson, J. Noteboom, K. C. O'briant, A. Allen, D. W. Lin, N. Urban, C. W. Drescher, B. S. Knudsen, D. L. Stirewalt, R. Gentleman, R. L. Vessella, P. S. Nelson, D. B. Martin, M. Tewari, *Proc. Natl. Acad. Sci. USA* **2008**, *105*, 10513.
[13] J. D. Arroyo, J. R. Chevillet, E. M. Kroh, I. K. Ruf, C. C. Pritchard, D. F. Gibson, P. S. Mitchell, C. F. Bennett, E. L. Pogosova-Agadjanyan, D. L. Stirewalt, J. F. Tait, M. Tewari, *Proc. Natl. Acad. Sci. USA* **2011**, *108*, 5003.
[14] G. B. Andersen, J. Tost, *Recent Results Cancer Res.* **2020**, *215*, 277.
[15] J. Zhang, S. Li, L. Li, M. Li, C. Guo, J. Yao, S. Mi, *Genomics, Proteomics Bioinf.* **2015**, *13*, 17.
[16] G. Raposo, W. Stoorvogel, *J. Cell Biol.* **2013**, *200*, 373.
[17] R. Kalluri, V. S. LeBleu, *Science* **2020**, *367*, eaau6977.
[18] Z. Zhao, J. Fan, Y. M. S. Hsu, C. J. Lyon, B. Ning, T. Y. Hu, *Lab Chip* **2019**, *19*, 1114.
[19] J. Chen, C. Hu, P. Pan, *Front. Physiol.* **2017**, *8*, https://doi.org/10.3389/fphys.2017.01028.
[20] J. Mills, M. Capece, E. Cocucci, A. Tessari, D. Palmieri, *Int. J. Mol. Sci.* **2019**, *20*, 6109.
[21] A. Thind, C. Wilson, *J. Extracell. Vesicles* **2016**, *5*, 31292.
[22] J. R. Chevillet, Q. Kang, I. K. Ruf, H. A. Briggs, L. N. Vojtech, S. M. Hughes, H. H. Cheng, J. D. Arroyo, E. K. Meredith, E. N. Gallichotte, E. L. Pogosova-Agadjanyan, C. Morrissey, D. L. Stirewalt, F. Hladik, E. Y. Yu, C. S. Higano, M. Tewari, *Proc. Natl. Acad. Sci. USA* **2014**, *111*, 14888.
[23] R. M. Graybill, R. C. Bailey, *Anal. Chem.* **2016**, *88*, 431.
[24] A. T. Sage, J. D. Besant, B. Lam, E. H. Sargent, S. O. Kelley, *Acc. Chem. Res.* **2014**, *47*, 2417.
[25] C. G. Liu, G. A. Calin, S. Volinia, C. M. Croce, *Nat. Protoc.* **2008**, *3*, 563.
[26] O. D. Murillo, W. Thistlethwaite, J. Rozowsky, S. L. Subramanian, R. Lucero, N. Shah, A. R. Jackson, S. Srinivasan, A. Chung, C. D.

Laurent, R. R. Kitchen, T. Galeev, J. Warrell, J. A. Diao, J. A. Welsh, K. Hanspers, A. Riutta, S. Burgstaller-Muehlbacher, R. V. Shah, A. Yeri, L. M. Jenkins, M. E. Ahsen, C. Cordon-Cardo, N. Dogra, S. M. Gifford, J. T. Smith, G. Stolovitzky, A. K. Tewari, B. H. Wunsch, K. K. Yadav, et al., *Cell* **2019**, *177*, 463.
[27] R. E. Crossland, J. Norden, L. A. Bibby, J. Davis, A. M. Dickinson, *J. Immunol. Methods* **2016**, *429*, 39.
[28] K. Boriachek, M. N. Islam, A. Möller, C. Salomon, N. T. Nguyen, M. S. A. Hossain, Y. Yamauchi, M. J. A. Shiddiky, *Small* **2018**, *14*, 1702153.
[29] J. H. Lee, J. A. Kim, S. Jeong, W. J. Rhee, *Biosens. Bioelectron.* **2016**, *86*, 202.
[30] L. Liu, H. Lu, R. Shi, X. X. Peng, Q. Xiang, B. Wang, Q. Q. Wan, Y. Sun, F. Yang, G. J. Zhang, *Anal. Chem.* **2019**, *91*, 13198.
[31] H.-L. Cheng, C.-Y. Fu, W.-C. Kuo, Y.-W. Chen, Y.-S Chen, Y.-M. Lee, K.-H. Li, C. Chen, H.-P. Ma, P.-C. Huang, Y.-L. Wang, G.-B. Lee, *Lab Chip* **2018**, *18*, 2917.
[32] Y. Yang, E. Kannisto, G. Yu, M. E. Reid, S. K. Patnaik, Y. Wu, *ACS Appl. Mater. Interfaces* **2018**, *10*, 43375.
[33] D. Taller, K. Richards, Z. Slouka, S. Senapati, R. Hill, D. B. Go, H.-C. Chang, *Lab Chip* **2015**, *15*, 1656.
[34] M. K. Masud, R. G. Mahmudunnabi, N. B. Aziz, C. H. Stevens, D. Do-Ha, S. Yang, I. P. Blair, M. S. A. Hossain, Y. B. Shim, L. Ooi, Y. Yamauchi, M. J. A. Shiddiky, *ChemElectroChem* **2020**, *7*, 3459.
[35] S. C. Chapin, P. S. Doyle, *Anal. Chem.* **2011**, *83*, 7179.
[36] H. Lee, S. J. Shapiro, S. C. Chapin, P. S. Doyle, *Anal. Chem.* **2016**, *88*, 3075.
[37] M. B. Nagarajan, A. M. Tentori, W. C. Zhang, F. J. Slack, P. S. Doyle, *Anal. Chem.* **2018**, *90*, 10279.
[38] D. C. Pregibon, P. S. Doyle, *Anal. Chem.* **2009**, *81*, 4873.
[39] D. Dendukuri, S. S. Gu, D. C. Pregibon, T. A. Hatton, P. S. Doyle, *Lab Chip* **2007**, *7*, 818.
[40] S. C. Chapin, D. C. Appleyard, D. C. Pregibon, P. S. Doyle, *Angew. Chem., Int. Ed.* **2011**, *50*, 2289.
[41] M. M. Ali, F. Li, Z. Zhang, K. Zhang, D. K. Kang, J. A. Ankrum, X. C. Le, W. Zhao, *Chem. Soc. Rev.* **2014**, *43*, 3324.
[42] M. A. Rider, S. N. Hurwitz, D. G. Meckes, *Sci. Rep.* **2016**, *6*, 23978.
[43] I. Helwa, J. Cai, M. D. Drewry, A. Zimmerman, M. B. Dinkins, M. L. Khaled, M. Seremwe, W. M. Dismuke, E. Bieberich, W. D. Stamer, M. W. Hamrick, Y. Liu, *PLoS One* **2017**, *12*, e0170628.
[44] Z. Andreu, E. Rivas, A. Sanguino-Pascual, A. Lamana, M. Marazuela, I. González-Alvaro, F. Sánchez-Madrid, H. de la Fuente, M. Yáñez-Mó, *J. Extracell. Vesicles* **2016**, *5*, 31655.
[45] D. Yang, W. Zhang, H. Zhang, F. Zhang, L. Chen, L. Ma, L. M. Larcher, S. Chen, N. Liu, Q. Zhao, P. H. L. Tran, C. Chen, R. N. Veedu, T. Wang, *Theranostics* **2020**, *10*, 3684.
[46] A. V. Vlassov, M. Li, E. Zeringer, R. Conrad, *US008901284B2* **2014**.
[47] F. Liu, O. Vermesh, V. Mani, T. J. Ge, S. J. Madsen, A. Sabour, E.-C. Hsu, G. Gowrishankar, M. Kanada, J. V. Jokerst, R. G. Sierra, E. Chang, K. Lau, K. Sridhar, A. Bermudez, S. J. Pitteri, T. Stoyanova, R. Sinclair, V. S. Nair, S. S. Gambhir, U. Demirci, *ACS Nano* **2017**, *11*, 10712.
[48] W. D. Gray, A. J. Mitchell, C. D. Searles, *MethodsX* **2015**, *2*, 360.
[49] P. Li, M. Kaslan, S. H. Lee, J. Yao, Z. Gao, *Theranostics* **2017**, *7*, 789.
[50] G. Gunkel, W. T. S. Huck, *J. Am. Chem. Soc.* **2013**, *135*, 7047.
[51] S. P. Jonstrup, J. Koch, J. Kjems, *RNA* **2006**, *12*, 1747.
[52] E. Schopf, Y. Chen, *Anal. Biochem.* **2010**, *397*, 115.
[53] J. Kim, J. S. Shim, B. H. Han, H. J. Kim, J. Park, I.-J. Cho, S. G. Kang, J. Y. Kang, K. W. Bong, N. Choi, *Biosens. Bioelectron.* **2021**, *192*, 113504.
[54] Q. Guo, F. Bian, Y. Liu, X. Qu, X. Hu, Q. Sun, *Chem. Commun.* **2017**, *53*, 4954.
[55] Q. Guo, Y. Yu, H. Zhang, C. Cai, Q. Shen, *Anal. Chem.* **2020**, *92*, 5302.
[56] V. Del Vescovo, M. Grasso, M. Barbareschi, M. A. Denti, *World J. Clin. Oncol.* **2014**, *5*, 604.
[57] S. Müller, F. Janke, S. Dietz, H. Sültmann, in *Tumor Liquid Biopsies*, Vol. 215 (Eds: F. Schaffner, J.-L. Merlin, N. von Bubnoff), Springer International Publishing, Cham **2020**, pp. 299–318.
[58] C. A. Raabe, T. H. Tang, J. Brosius, T. S. Rozhdestvensky, *Nucl. Acids Res.* **2014**, *42*, 1414.
[59] S. Srinivasan, A. Yeri, P. S. Cheah, A. Chung, K. Danielson, P. De Hoff, J. Filant, C. D. Laurent, L. D. Laurent, R. Magee, C. Moeller, V. L. Murthy, P. Nejad, A. Paul, I. Rigoutsos, R. Rodosthenous, R. V. Shah, B. Simonson, C. To, D. Wong, I. K. Yan, X. Zhang, L. Balaj, X. O. Breakefield, G. Daaboul, R. Gandhi, J. Lapidus, E. Londin, T. Patel, R. L. Raffai, et al., *Cell* **2019**, *177*, 446.
[60] S. R. Pfeffer, K. F. Grossmann, P. B. Cassidy, C. H. Yang, M. Fan, L. Kopelovich, S. A. Leachman, L. M. Pfeffer, *J. Clin. Med.* **2015**, *4*, 2012.
[61] G. K. Joshi, S. Deitz-McElyea, T. Liyanage, K. Lawrence, S. Mali, R. Sardar, M. Korc, *ACS Nano* **2015**, *9*, 11075.
[62] Y. Pang, C. Wang, L. C. Lu, C. Wang, Z. Sun, R. Xiao, *Biosens. Bioelectron.* **2019**, *130*, 204.
[63] N. W. Choi, J. Kim, S. C. Chapin, T. Duong, E. Donohue, P. Pandey, W. Broom, W. A. Hill, P. S. Doyle, *Anal. Chem.* **2012**, *84*, 9370.